Cell Stem Cell
Article

Accumulating Mitochondrial DNA Mutations Drive Premature Hematopoietic Aging Phenotypes Distinct from Physiological Stem Cell Aging

Gudmundur L. Norddahl,[1] Cornelis J. Pronk,[1] Martin Wahlestedt,[1] Gerd Sten,[1,2] Jens M. Nygren,[1,3] Amol Ugale,[1] Mikael Sigvardsson,[4] and David Bryder[1,2,*]
[1]Immunology Section, Institution for Experimental Medical Science, BMC D14, Lund University, Tornavägen 10, 221 84 Lund, Sweden
[2]Lund Strategic Research Center for Stem Cell Biology and Cell Therapy, Lund University, Box 117, SE-221 00 Lund, Sweden
[3]Center of Research on Welfare, Health and Sport, Halmstad University, PO Box 823, 301 18 Halmstad, Sweden
[4]Institution of Clinical and Experimental Medicine, Linköping University, Sandbäcksgatan 7, 581 83, Linköping, Sweden
*Correspondence: david.bryder@med.lu.se
DOI 10.1016/j.stem.2011.03.009

SUMMARY

Somatic stem cells mediate tissue maintenance for the lifetime of an organism. Despite the well-established longevity that is a prerequisite for such function, accumulating data argue for compromised stem cell function with age. Identifying the mechanisms underlying age-dependent stem cell dysfunction is therefore key to understanding the aging process. Here, using a model carrying a proof-reading-defective mitochondrial DNA polymerase, we demonstrate hematopoietic defects reminiscent of premature HSC aging, including anemia, lymphopenia, and myeloid lineage skewing. However, in contrast to physiological stem cell aging, rapidly accumulating mitochondrial DNA mutations had little functional effect on the hematopoietic stem cell pool, and instead caused distinct differentiation blocks and/or disappearance of downstream progenitors. These results show that intact mitochondrial function is required for appropriate multilineage stem cell differentiation, but argue against mitochondrial DNA mutations per se being a primary driver of somatic stem cell aging.

INTRODUCTION

The hematopoietic system experiences several age-associated alterations with profound consequences for health, including reduced immune competence, anemia, and an increased propensity for hematopoietic cancers (Rossi et al., 2008). In addition, graft age is by far the most significant negative parameter in bone marrow transplantation (Kollman et al., 2001), which represents perhaps the best example of how age can compromise and influence therapeutic approaches based on regenerative medicine. Several studies have highlighted that intrinsic molecular differences underlie alterations in HSC function with age (Rossi et al., 2008). This fact has developed our understanding of the manifestations of the aging blood system and include an HSC intrinsic loss of differentiation capacity to the lymphoid lineages and a perturbed reconstitution capacity with age (Beerman et al., 2010), thereby suggesting HSCs as prime cellular targets in therapeutic strategies aimed at minimizing the shortcomings of hematopoietic aging.

While extensive data have been presented on the phenotypes that associate with hematopoietic aging, less is known about its underlying cause. The mitochondria of mammalian cells uphold cellular function and survival by several key processes, which include oxidative phosphorylation (OXPHOS), various metabolic processes, and apoptosis. As a remnant of once being symbiotic bacteria living within early eukaryotes, mitochondria carry their own genome. This small genome (≈16 kb) is replicated independently from the nuclear genome and constitutes 37 genes; 13 for subunits of respiratory complexes, 22 tRNAs, and two rRNAs (Falkenberg et al., 2007). During evolution, remaining genes necessary for appropriate mitochondrial function have been transferred or exchanged for homologous genes in the nucleus, the products subsequently being imported into the mitochondria to mediate their functions. These include all the genes of the mitochondrial replication machinery (Falkenberg et al., 2007). Inherent disorders of mitochondria underlie several known disruptions in metabolism and can result in dramatic impairment of organismal health. In the hematopoietic system, dysfunctional mitochondria have been reported to be associated with malignant transformation, myelodysplastic syndrome, and Pearson's syndrome, as well as more defined genetic disorders such as X-linked sideroblastic anemia (Fontenay et al., 2006).

Aberrant mitochondrial function might also be particularly relevant in aging because most, if not all, tissues investigated thus far experience an age-dependent accumulation of mitochondrial DNA (mtDNA) mutations (Larsson, 2010). The demonstration that multiple aspects of aging were accelerated in "mutator" mice harboring error-prone forms of the mitochondrial DNA polymerase gamma (POLG) (Kujoth et al., 2005; Trifunovic et al., 2004) provided direct support for a mitochondrial theory of aging. However, while these mutator strains presented phenotypes mimicking premature aging, there is less information about the direct cellular targets and the fundamental issue of how accumulating mtDNA mutations might affect somatic stem cell fate.

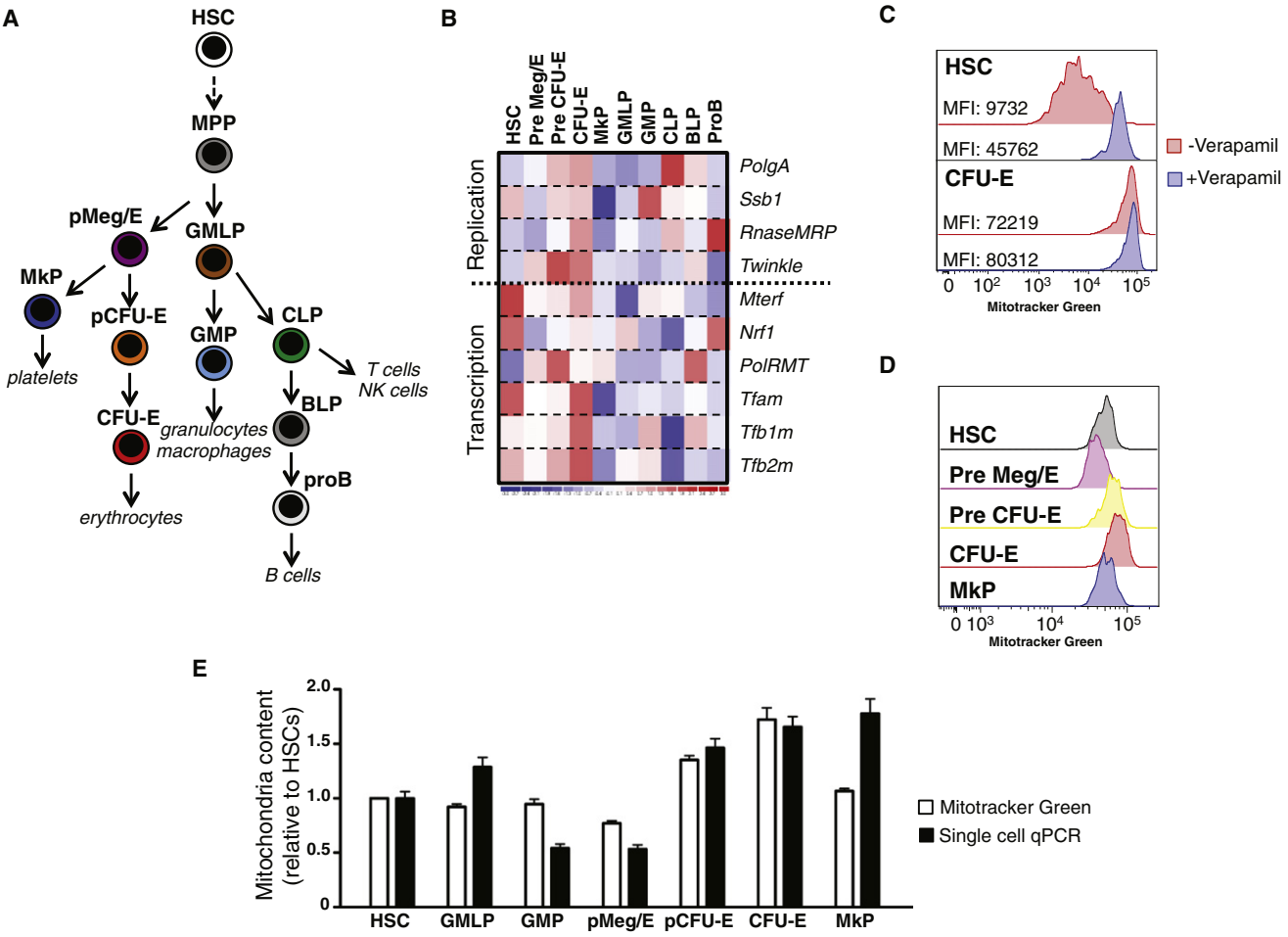

Figure 1. Mitochondria Regulation in Early Hematopoietic Differentiation

(A) Schematic representation of hematopoietic development depicting the progenitor cell types characterized in this study.

(B) Heat-map display of RNA expression for key nuclear-encoded mitochondrial-associated genes. Red indicates high while blue indicates low expression in the indicated cell types (expression levels normalized for each gene across cell types).

(C) Representative MTG profiles of indicated progenitor cells in the absence or presence of Verapamil (MFI; mean fluorescence intensity) (n = 3).

(D) MTG profiles of indicated cell subsets performed in the presence of Verapamil.

(E) Comparison of MTG profiles and single cell mtDNA qPCRs of indicated progenitors. Open bars: relative MTG MFI (n = 3). Filled bars: relative single cell mtDNA content in indicated progenitors (n = 89 of each subset). Data were normalized to HSCs and displayed as mean ± SEM.

See also Figures S1 and S4.

To explore the consequences of accumulating mtDNA mutations for the blood system, we performed an extensive characterization of the alterations in hematopoietic stem and progenitor cell phenotypes and functions in POLG mutator mice. We demonstrate a severe compromise in early lymphoid and erythroid development from mutator HSCs, and identify precise cellular stages where these deficits arise. Surprisingly, these apoptosis-associated phenotypes were initially independent of HSC self-renewal and myeloid cell differentiation/proliferation; the latter, which require continuous production from HSCs due to their high turnover (Domen et al., 2000). In agreement with these stage-specific effects, global gene expression studies of mutator HSCs failed to mimic the molecular alterations that associate with normal HSC aging (Chambers et al., 2007; Rossi et al., 2005), with clear alterations in mitochondrial membrane potential being restricted to affected progenitors. Although stressed mutator HSCs, provoked either by serial transplantation or chronologic age, also severely blunted HSC self-renewal, their magnitude never approached that observed for lymphopoiesis and erythropoiesis. Thereby, our studies highlight the critical requirement of mitochondrial integrity for multilineage hematopoiesis, but segregate normal HSC aging from the primary consequences of accumulating mtDNA mutations.

RESULTS

Evidence for Differential Mitochondrial Regulation in Early Hematopoietic Differentiation

To begin to detail mitochondrial regulation at distinct stages of hematopoietic differentiation (Figure 1A), we first investigated the RNA expression patterns of a core set of nuclear genes with established roles in mitochondrial DNA (mtDNA) replication

and transcription (Figure 1B). Overall, this demonstrated higher expression of such genes in early erythroid committed progenitors (Figure 1B), although significant expression levels were observed throughout the investigated cellular stages. Importantly, these data indicated ongoing mitochondrial regulation in HSCs, despite the recent observations that HSCs rely more on anaerobic rather than aerobic respiration for energy metabolism (Simsek et al., 2010).

We next investigated mitochondria directly by staining defined hematopoietic progenitor subsets (Figure 1A) with the fluorescent dye Mitotracker Green (MTG), followed by FACS analysis. MTG localizes to mitochondria regardless of mitochondrial membrane potential (MMP), and can be used to enumerate the mitochondrial content in intact cells. However, since MTG has been reported to be a substrate for multi drug resistance (MDR) activity (Marques-Santos et al., 2003), we initially examined the effects of Verapamil, an MDR blocker, on MTG uptake. This revealed a critical requirement of blocking MDR activity for efficient MTG uptake, a feature particularly evident in HSCs (Figure 1C and see Figure S1A available online), which are known to exhibit high MDR activity (Chaudhary and Roninson, 1991; Goodell et al., 1997).

MTG staining (in the presence of Verapamil) revealed that the mitochondrial content was reduced in the transition of HSCs to bipotent megakaryocytic/erythroid precursor cells (pre Meg/Es) but gradually increased upon differentiation through the erythroid committed progenitors pre CFU-Es and CFU-Es (Figure 1D). Next, to complement the MTG analyses with an independent method, we quantified mtDNA in a large spectrum of hematopoietic progenitor cells by single-cell quantitative PCR (qPCR) (Figure 1E). Although slightly discrepant with the MTG profiles for some of the investigated cell types (i.e., GMP and MkP), these methods gave highly similar results for most of the investigated cell types (Figure 1E). Finally, we also performed qPCR on mtDNA from hematopoietic progenitors sorted in bulk and normalized for the quantity of genomic DNA (Wong and Cortopassi, 2002) (Figure S1B), which is a more traditional, although slightly suboptimal, method for the specific purpose here, given its dependence on nuclear gene normalization and the highly varying cell cycle status among different progenitor cell subsets (Passegue et al., 2005). Taken together, these experiments revealed dynamic changes in mtDNA content upon HSC differentiation, and importantly demonstrated a relatively high mitochondrial content of HSCs, a cell type otherwise characterized by low MMP (Simsek et al., 2010).

Accumulating Mitochondrial Mutations Cause Progressive and Selective Perturbations in Early Hematopoiesis Distinct from Normal Aging

We next wanted to investigate the hematopoietic dependence on intact mitochondrial function. To this end, we took advantage of a mouse strain engineered to express a proofreading-defective form of POLG (Trifunovic et al., 2004), referred to hereafter as mutator mice.

We first investigated the hematopoietic progenitor cell composition of mutator mice and their littermate controls. The cellular composition of hematopoietic cells in BM and periphery of young mutator mice (9–12 weeks) were indistinguishable from their heterozygous or wild-type littermate controls (GLN and DB, data not shown) (Chen et al., 2009; Figure S2). By contrast, intermediately aged (33–36 weeks old) mutator mice displayed pronounced alterations in several hematopoietic progenitor cell compartments (Figure 2), which extended to mature effector cells (Figure S2). While no changes were observed in the frequency of HSCs (Figure 2A), mutator mice presented a striking increase of pre Meg/Es (5.8-fold) and pre CFU-Es (24.5-fold) (Figures 2B and 2C). To allow for correlation to more advanced age, we conducted similar analysis on 100-week-old mice, although this precluded evaluation of mutator mice that do not reach this age (Trifunovic et al., 2004). In sharp contrast to intermediately aged mutator mice, advanced aged WT mice did not display an accumulation of either pre Meg/Es or pre CFU-Es (Figures 2B and 2C), but exhibited pronounced increases in HSC numbers, in agreement with previous studies (Rossi et al., 2005). These data established that the defect in erythropoiesis observed in mutator mice (Chen et al., 2009; Trifunovic et al., 2004; Figure S2) associated with a severe differentiation block at defined stages of early erythroid development (Figure 2C), which segregated from normal physiologic aging (Figures 2B and 2C).

Apart from defective erythropoiesis, mutator mice have also been reported to display perturbations in lymphopoiesis in an age-dependent manner (Chen et al., 2009). However, in contrast to erythropoiesis, where the earliest stages of development were affected (Figures 2B and 2C), the most primitive lymphoid-restricted populations remained unaffected with intact frequencies of common lymphoid progenitors (CLPs), B cell-biased lymphoid progenitors (BLP) (Inlay et al., 2009), and Pre/ProB cells (Figure 2D). This was strikingly different from the physiologically aged setting, which was characterized by reduced frequencies of all these progenitors (Figure 2D). By contrast, ProB cells (defined by a $B220^{+}CD19^{+}IL7Ra^{+}$ phenotype) were dramatically reduced in intermediately aged mutator mice, while $B220^{+}CD19^{+}IL7Ra^{-}$ cells, which include recirculating B cells, were less affected (Figures 2E and 2F). Again, aged WT contrasted these phenotypes (Figures 2E and 2F).

Mitochondrial DNA Mutations Compromise the Multilineage and Self-Renewal Capacity of Hematopoietic Stem Cells in an Asynchronous Manner

To assess HSC function of mutator mice, we isolated and transplanted candidate HSCs from young CD45.1 mutator mice or their littermate controls into young CD45.2 wild-type mice. To allow quantification, we performed these experiments in a competitive manner (Harrison, 1980). Test-cell-derived reconstitution was observed in all recipients regardless of their genotype (Figure 3A). HSCs from wild-type mice efficiently supported high levels of long-term reconstitution of all blood cell lineages. By contrast, severe perturbations were observed in the ability of mutator HSCs to repopulate the B and T cell lineages (Figure 3A), although, importantly, all recipients of mutator HSCs contained some levels of donor-derived B and T cells. Heterozygous mutator HSCs displayed an intermediate phenotype (Figure 3A), suggesting a gene dosage effect in this setting.

It is well known that transplantation enforces enhanced HSC cycling (Allsopp et al., 2001) and serial transplantation can therefore be used to expose genetic phenotypes with subtle HSC phenotypes in the steady state, since this eventually

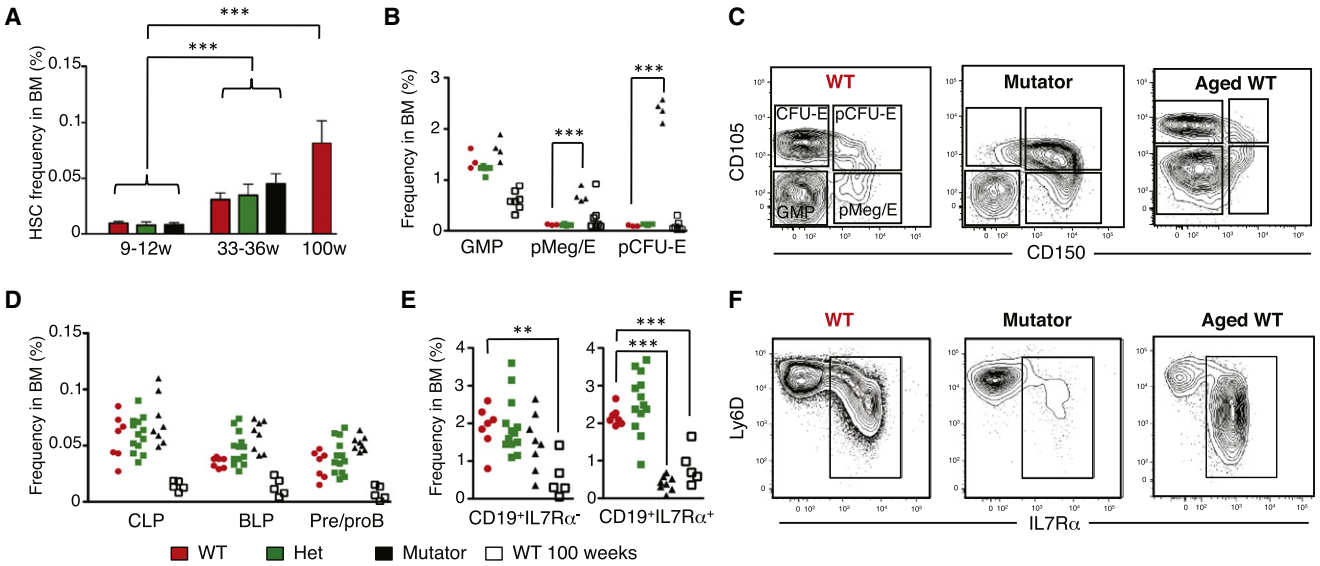

Figure 2. Mitochondria Mutations Alter the Hematopoietic Differentiation Capacity of Mutator Mice in a Time-Dependent Manner, but are Distinct from Normal Hematopoietic Aging

(A) HSC frequencies in 9- to 12-week-old and 33- to 36-week-old wild-type, heterozygous, or homozygous mutator and aged wild-type (100 weeks) bone marrow (mean values ± SEM, n = 3–5).

(B) Myeloid progenitor cell frequencies in 33- to 36-week-old and 100-week-old mice of indicated genotypes (data points refer to frequencies in individual mice).

(C) Representative FACS plots of myeloid progenitors in bone marrow of 33- to 36-week-old wild-type (left panel), mutator mice (middle panel), and aged WT mice (100 weeks) (right panel), which highlight the pronounced accumulation of mutator pre CFU-E cells.

(D) Lymphoid progenitor frequencies measured by FACS in mid-aged and aged mice (100 weeks) of indicated genotypes, with each data point referring to values in individual mice.

(E) B cell restricted progenitor frequencies (pre-gated on $B220^{+}CD19^{+}$ cells) in mid-aged and aged mice of indicated genotypes, with each data point referring to values in individual mice.

(F) FACS plots illustrating the decrease of $IL7Ra^{+}$ ProB cells (boxed) in mutator mice.

See also Figure S2.

exhausts the HSC function even of wild-type HSCs (Harrison et al., 1978). This was especially relevant in the context of the mutator model, as the hematopoietic phenotypes of these mice arise in a strict time-dependent manner in steady state (Figure 2 and Figure S2). We used a strategy where 1×10^6 young WT or mutator $CD45^{+}$ BM cells were transplanted noncompetitively into a set of lethally irradiated WT hosts. From these primary hosts, we isolated donor-derived HSCs 16 weeks after transplantation and transferred these cells into lethally irradiated secondary hosts in competition with WT BM cells. In this setting, mutator HSCs exhibited a 6.7-fold lower contribution to mature blood cells as compared to the transplanted WT cells (Figure 3B). We also conducted experiments where mid-aged WT or mutator HSCs were isolated and competitively transplanted into lethally irradiated hosts. The observed phenotype of mutator HSCs in this setting (Figure 3C) was highly reminiscent of serially transplanted mutator HSCs (Figure 3B).

Mature peripheral erythrocytes do not express the CD45 marker that is used to distinguish between test and competitor/host-derived blood cells of other lineages. Thus, to expose potential alterations in the erythroid lineage in the primary transplantation setting, we turned our attention to the bone marrow where immature erythroid progenitors express detectable levels of the CD45 marker up to the CFU-E stage. These analyses revealed that mutator-derived erythroid progenitor reconstitution (pre CFU-Es and CFU-Es) was strongly diminished (2.8-fold; Figure 3D) 16 weeks after transplantation, demonstrating that the HSC defects of mutator mice include the erythroid lineage (Figure 3D). We next sought to directly confirm the ongoing HSC self-renewal. To this end, HSC recipients were sacrificed 16 weeks after transplantation to allow for an investigation of the HSC-derived progenitor compartments. These data demonstrated an indistinguishable regeneration of mutator HSCs as compared to their littermate controls (Figure 3D). Upon extensive proliferation caused by serial transplantation of mutator HSCs, there is a further decline in their erythroid potential while retention of an apparent, although reduced, capacity to self-renew (Figure 3E). The dependence of intact mitochondrial function for appropriate lympho- and erythropoiesis could be extended also to an in vitro situation (Figure S3).

Taken together, these data demonstrate that the hematopoietic lineage defects in mutator mice are caused by functional alterations in lineage-restricted progenitor cells rather than at the level of HSCs. However, extensive proliferation of mutator HSCs upon regenerative stress and aging ultimately cause a functional decline also in HSC self-renewal.

The Consequences of Accumulating Mitochondrial DNA Mutations for Mitochondrial Function

Because of the maintained HSC activity of mutator mice, despite the severe functional compromise at downstream progenitor levels, we next directly evaluated the mtDNA mutation rates in

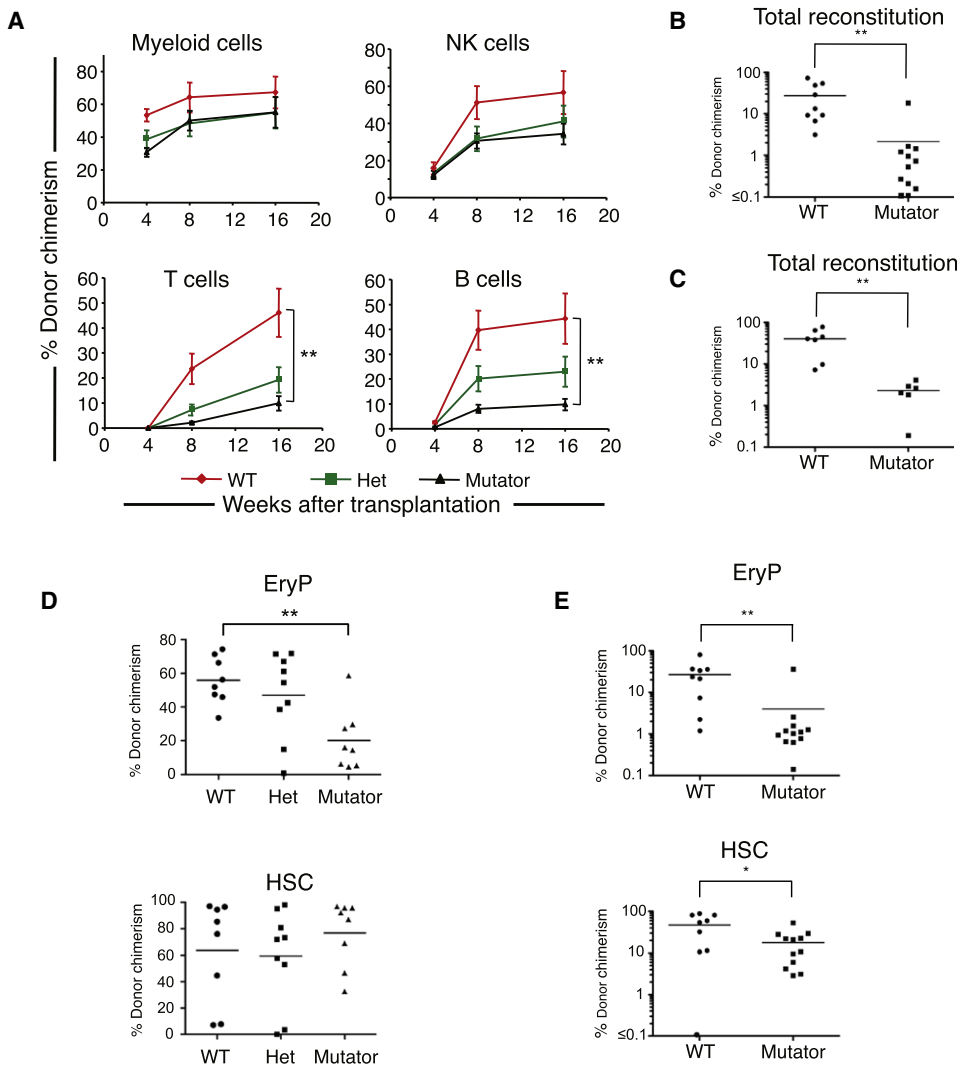

Figure 3. The Altered Hematopoiesis of Mutator Mice has a Hematopoietic Stem Cell Autonomous Origin

(A) One hundred Lin$^-$ckit$^+$Sca1$^+$CD34$^{-/lo}$Flt3$^-$CD150$^+$ cells isolated from mutator mice or littermates (CD45.1) were transplanted per mouse into lethally irradiated C57BL/6 WT mice (CD45.2), together with a competitive dose of 300,000 unfractionated C57BL/6 bone marrow cells. Peripheral blood was analyzed for donor contribution at given time points (mean ± SEM, n = 8 to 9 recipients per group).

(B) 10^6 unfractionated BM cells from mutator cells or their wild-type littermate controls were used to reconstitute the blood system of primary lethally irradiated C57BL/6 hosts. Long-term after transplantation (16 weeks), HSCs (Lin$^-$ckit$^+$Sca1$^+$CD34$^{-/lo}$Flt3$^-$CD150$^+$) were isolated from the bone marrow of primary recipients, after which they were transplanted at 500 cells/mouse together with 300,000 C57Bl/6 unfractionated bone marrow cells. Shown is the total contribution in individual mice 16 weeks post-transplantation, with reference lines indicating the group mean.

(C) Five hundred Lin$^-$Sca1$^+$ckit$^+$CD150$^+$CD48$^-$ isolated from aged mutator mice or littermates (33 to 34 weeks) were transplanted competitively into lethally irradiated WT recipient mice. Shown is the total contribution in individual mice 16 weeks post-transplantation, with reference lines indicating the group mean.

(D) Donor contribution to the erythroid and HSC progenitor pools in bone marrow 6 months after primary transplantation. Data show individual recipients with reference lines indicating group mean value.

(E) Donor contribution to the erythroid and HSC progenitor pools in bone marrow 6 months after initiation of secondary transplantations. Data show levels in individual mice, with reference lines indicating group mean value.

See also Figure S3.

HSCs. For comparison, we also evaluated mutation rates in pre CFU-Es, a cell type severely affected in mutator mice. To obtain sufficient sequencing depth, we PCR-amplified mtDNA fragments from single-sorted HSCs and pre CFU-Es (Figure 4A). While the majority of the mtDNA mutations were heteroplasmic (Figure 4A, left panel), the results further demonstrated higher and similar mutation frequencies of both mutator HSCs and pre CFU-Es compared to their littermate control cells. Thus, HSCs in mutator mice display comparable levels of mutations as their downstream progeny.

To begin to unravel the functional consequences of increased mtDNA mutations on the phenotypes of hematopoietic subpopulations, we next determined the effect of increased mtDNA mutation load on mitochondrial membrane potential (MMP) by

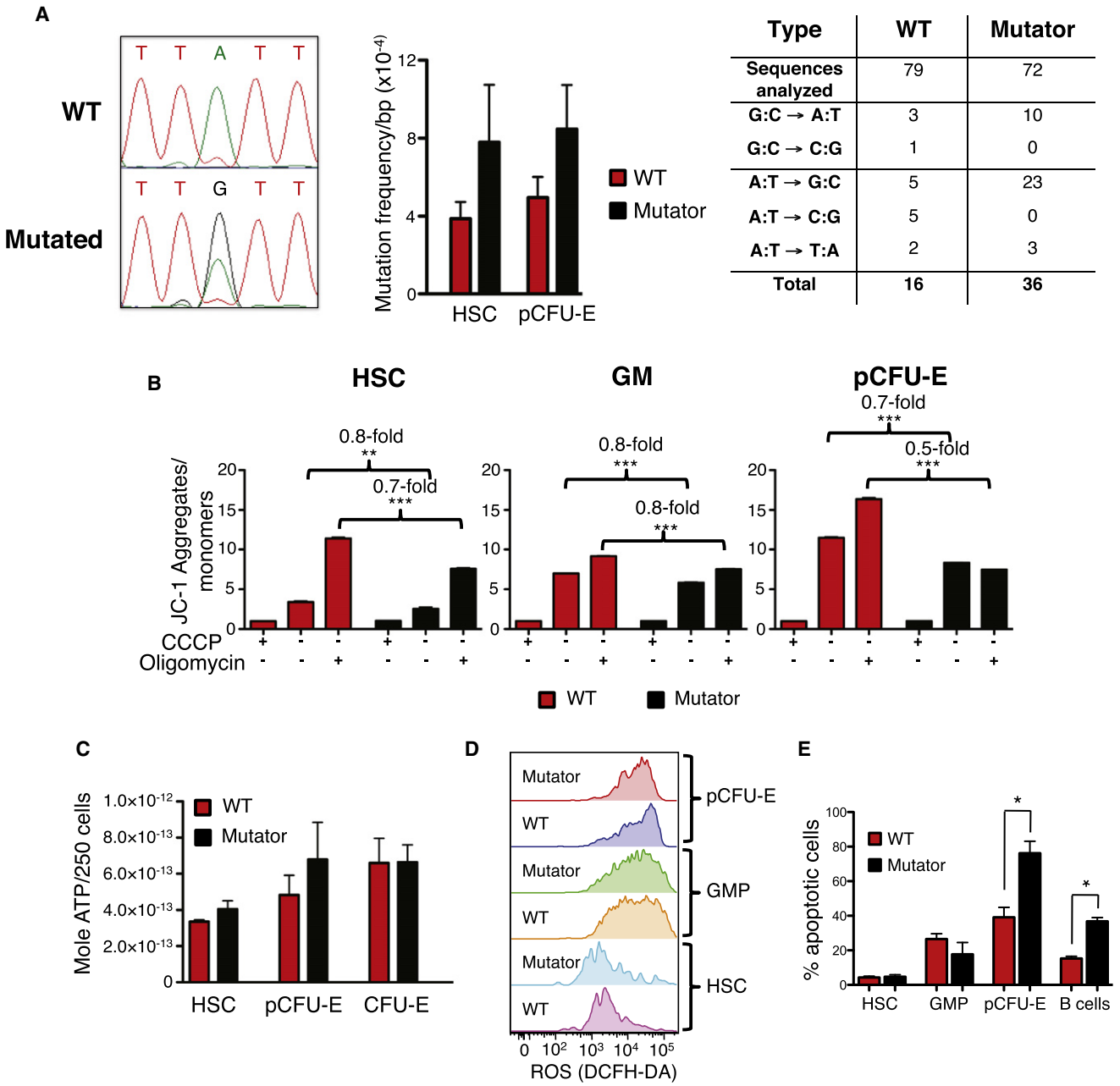

Type	WT	Mutator
Sequences analyzed	79	72
G:C → A:T	3	10
G:C → C:G	1	0
A:T → G:C	5	23
A:T → C:G	5	0
A:T → T:A	2	3
Total	16	36

Figure 4. Hematopoietic Progenitor Cells from Mutator Mice Display with Increased Mitochondrial DNA Mutation Loads and Altered Mitochondrial Membrane Potential Leading to Lineage Specific Increases in Apoptosis

(A) Single HSCs and pre CFU-Es were sorted from WT and mutator mice (30 weeks old) into lysis buffer and subjected to PCR with primers directed against a portion of mitochondrial DNA, followed by sequencing (30–43 individual sequences obtained per cell type). Left panel: Representative sequence data. Note the heteroplasmic nature of mutation. Middle panel: Calculated mutation frequencies in the indicated progenitors (mean ± SEM). Right panel: Summary of mutation types.

(B) Indicated cell types were treated with the ion uncoupler CCCP that disrupts the mitochondria membrane potential or the F_0/F_1 ATPase inhibitor Oligomycin, as indicated. Displayed data are from one of three experiments with similar results (data show mean ± SEM).

(C) Two hundred and fifty HSCs and pre CFU-Es were isolated in triplicates from mutator and littermate mice (39 weeks) and subjected to ATP measurements (data show mean ± SEM, n = 3).

(D) Indicated progenitor cell subsets were evaluated for ROS levels by DCFH-DA staining and enumerated by FACS. Data show representative FACS plots of ROS levels in indicated progenitor subsets from mutator or control mice (29 weeks) (analysis performed on three mice/genotype).

(E) Indicated progenitor subsets were isolated and cultured (HSCs, GMPs, and pre CFU-Es were cultured for 3 days in suspension while GMLPs were cocultured with OP9 stromal cells for 11 days), followed by determination of the ratio of apoptotic cells by FACS following Annexin V and PI staining (data show mean ± SD from three to four mice/genotype).

JC-1 stainings of defined progenitor subsets. These experiments demonstrated that, regardless of genotype, HSCs displayed lower MMP than both GMs and pre CFU-Es, whereas pre CFU-Es showed the highest MMP (Figure 4B). Mutator HSCs, GMs, and pre CFU-Es all displayed slightly lower MMP compared to their WT counterparts (Figure 4B). As mitochondria sustain the MMP through the proton-transporting activity of the oxidative respiratory chain complexes (Huttemann et al., 2008), we speculated that decreased MMP was a result of reduced OXPHOS activity as has been previously been observed in skeletal muscle cells using an independent mutator strain (Hiona et al., 2010). To test this hypothesis, we treated cells with Oligomycin, an F_0-ATPase inhibitor that blocks the activity of Complex V of the oxidative phosphorylation chain, which results in accumulation of protons in the mitochondrial intermembrane space and therefore an increased MMP. Despite that both mutator HSCs and GMs displayed lower MMP than WT cells upon Oligomycin treatment, both these cell types showed similar increase in MMP compared to WT cells (Figure 4B). Strikingly, however, the mitochondria of mutator pre CFU-Es failed to raise the MMP to levels observed with WT progenitors (Figure 4B). Mitochondria of all cells investigated lost their membrane potential upon treatment with the ion uncoupler CCCP (Figure 4B).

As the mitochondrial proton gradient is harnessed for the synthesis of ATP, we speculated that the different MMP between the different progenitor subsets could have a differential dependence on ATP produced by OXPHOS. Since mutator pre CFU-Es displayed both a lowered MMP and an abnormal response to Oligomycin, we hypothesized that the observed differential block at this cellular stage was due to a defective ATP synthesis in these cells. Somewhat surprisingly however, mutator cells did not appear to exhibit different levels of intracellular ATP when compared to WT cells (Figure 4C). According to the mitochondrial theory of aging, mtDNA accumulates mutations due to oxidation by mitochondrial-derived ROS, an accumulation of mutations that augments further ROS production (Harman, 1972). However, in agreement with previous studies using in vitro cultured or other terminally differentiated cell types, we did not observe any difference in ROS levels between WT and mutator hematopoietic progenitor cells (Figure 4D).

Lowered MMP correlates with cells undergoing apoptosis, and cells overexpressing the antiapoptotic protein BCL-2 exhibit an increase in MMP (Gogvadze et al., 2006). We therefore next decided to investigate if we could find any evidence of elevated apoptosis rates of mutator cells. HSCs, GMPs, and pre CFU-Es were cultured for 3 days in suspension cultures, while GMLPs were cultured on OP9 stromal cells for 11 days in order to allow for B cell development. On the last day of culture, cells were harvested and stained with Annexin V and/or propidium iodide (PI) to measure apoptosis. These experiments revealed that HSCs display lower rates of apoptosis than other cell types, a feature independent of genotype (Figure 4E), further supporting our findings that HSCs remain mostly unaffected by the mutator genotype. In agreement with our transplantation data, both mutator and littermate GMPs exhibit comparable levels of apoptosis (Figure 4E). Strikingly however, mutator pre CFU-Es and B cells displayed an almost 2-fold increase of apoptotic cells (Figure 4E).

The Phenotypic and Molecular Features of Mutator Hematopoietic Stem Cells are Distinct from Normal Physiological Aging

The HSC compartment undergoes a range of functional and phenotypic alterations with age (Rossi et al., 2005). As mutator mice have been described as a model of premature aging, we therefore next set out to detail how well this correlated to the setting of physiological HSC aging.

A recently identified hallmark of normal HSC aging is an accumulation and striking dominance within the candidate HSC pool of a defined myeloid-biased subset of HSCs (Beerman et al., 2010). Such cells can be prospectively identified based on their high expression of Slamf1 (CD150). Given the myeloid-biased output from mutator mice and similarities shared with physiologically aged HSCs (Figure 5A), we investigated young (10–12 weeks), mid-aged (33 to 34 weeks), and aged (100 weeks) mutator and control mice for HSC subset composition. These experiments revealed a gradual age-dependent elevation in the myeloid-biased Slamf1^{hi} HSC subset (Figure 5B), independent of genotype. Thus, despite the pronounced myeloid-biased output of mutator HSCs (Figure 5A), only small differences were observed in HSC subset distribution (Figure 5C), while as previously reported (Beerman et al., 2010), physiological aging was associated with a striking dominance of the myeloid-biased Slamf1^{hi} HSC subset.

To further our comparison of mutator HSCs to those of physiologically aged HSCs, we next evaluated the ATP levels (Figure 5D), ROS production (Figure 5E), and MMP (Figure 5F) of young and aged WT HSCs. While none of these parameters were altered in aged HSCs, this was in contrast to mutator HSCs that showed a consistent reduction in MMP (Figure 4).

Although the mechanisms underlying HSC aging remain to be fully revealed, normally aged WT HSCs have a characteristic global gene expression signature (Chambers et al., 2007; Rossi et al., 2005). Because we, throughout these studies, used a slightly different phenotype to identify candidate HSCs compared to previous studies, and to further our analyses on potential similarities between normal physiologic aging and the premature aging phenotypes of mutator mice, we isolated RNA from candidate Lin$^-$Sca1$^+$ckit$^+$CD150$^+$CD48$^-$ HSCs sorted from young (9–12 weeks) and aged (>2 year old) WT mice and subjected it to Affymetrix 430.2 gene chip analysis. Next, we conducted similar experiments on RNA isolated from HSCs from mid-aged mutator mice or their wild-type littermate controls.

To define the shift in gene expression that associated with physiological HSC aging, we first analyzed the gene chip data for how many genes displayed a 2-fold change in expression in young WT HSCs compared to the aged WT HSCs. With this stringent criterion, 35 probe sets exhibited lower expression and 140 probe sets were upregulated in the aged HSCs, while 11,095 displayed less than a 2-fold difference (Figure 5G; Table S1). Next, we executed the same analysis on HSCs derived from the mutator and littermate mice. In striking contrast to normal HSC aging, this revealed only two genes to be either up- or downregulated in mutator HSCs (Figure 5G; Table S1). We also subjected our microarray data to Gene Set Enrichment Analysis, which is a method to determine whether defined gene sets might display statistically significant differences between

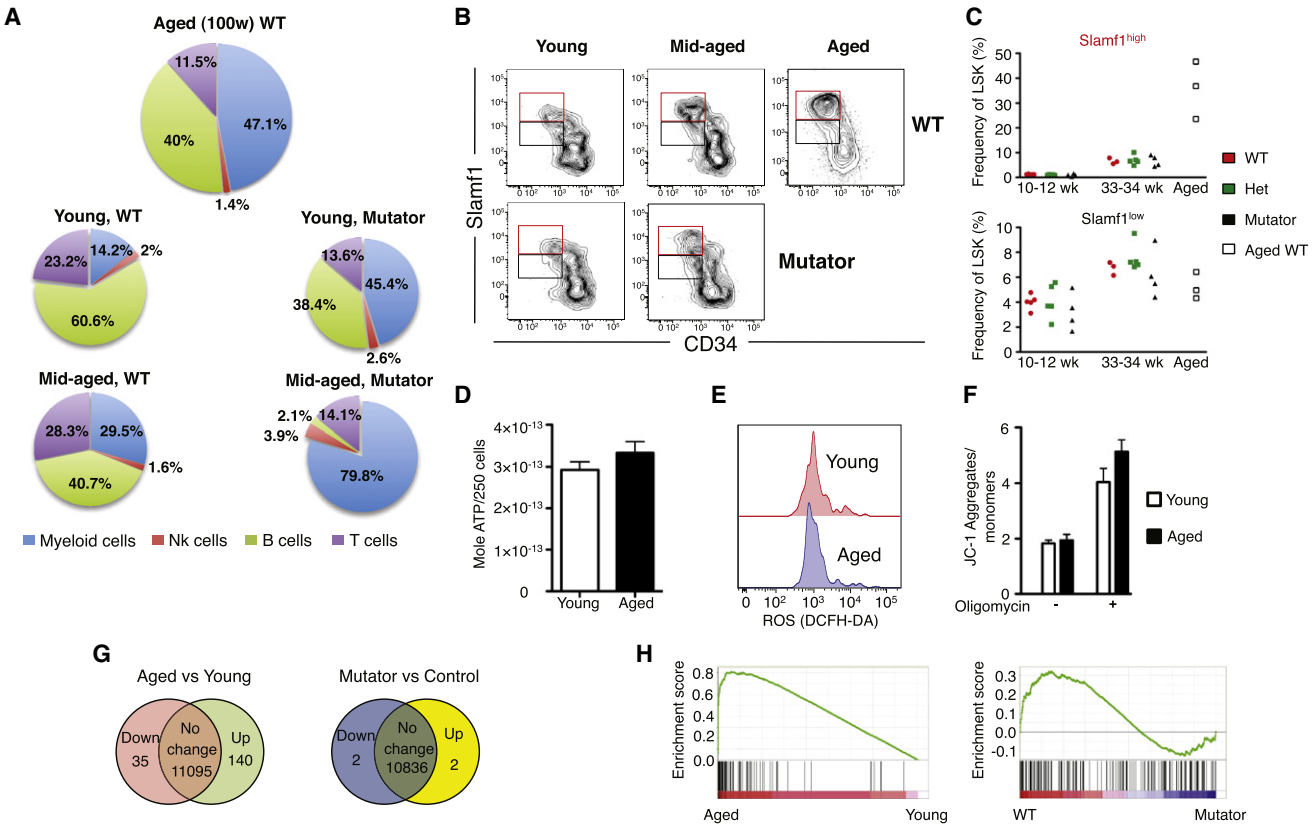

Figure 5. Hematopoietic Stem Cells of Mutator Mice; Fundamental Differences to the Setting of Physiologically Aging

(A) Lineage contribution following transplantation of mutator and WT HSCs at different ages. Pie charts show average contribution of HSCs from indicated sources to each indicated lineage 4 months after transplantation (n = 6–8 recipients/group).

(B) Representative FACS plots of bone marrow cells stained with antibodies against lineage antigens, Sca1, ckit, Flt3, CD150, and CD34 to identify myeloid-biased HSCs. Displayed are lineage$^-$Sca1$^+$ckit$^+$Flt3$^-$ pregated cells.

(C) Frequency enumeration of Slamf1^{hi} (myeloid-biased) and Slamf1^{lo} HSCs in individual mice.

(D) Two hundred and fifty HSCs from young (10–14 weeks) and aged (100 weeks) WT mice were subjected to ATP measurement (n = 3 mice for each genotype). Data show mean values ± SEM.

(E) Young (10–14 weeks) and aged (100 weeks) HSCs were evaluated for ROS levels by DCFH-DA staining. Representative FACS plots from three independent experiments.

(F) JC-1 staining of young (10–14 weeks) and aged (100 weeks) HSCs with or without Oligomycin. Data show mean values ± SEM (n = 3).

(G) RNA was extracted from sorted HSCs, followed by linear amplification, and hybridized to Affymetrix 430 2.0 arrays (triplicate arrays/condition). Venn diagrams are displayed with the number of genes that were 2-fold or higher differentially expressed in aged versus young WT HSCs and mutator (32 weeks) versus WT littermate HSCs (32 weeks), respectively.

(H) The 140 gene HSC aging-associated signature was assessed with GSEA for correlation to the expression profiles of aged versus young WT HSCs in an independent training set (left panel), and mutator versus littermate HSCs (right panel).

See also Table S1.

two biological states (Subramanian et al., 2005). The power of this method is based on the fact that it concentrates on gene sets that share a common biological property (in this case, age) instead of focusing merely on the difference between individual genes. Thus, this method should have the capacity to reveal subtler changes in gene expression that cannot be revealed by the stringent analysis criteria used in our primary analyses. We focused on the 140 genes that became upregulated upon physiological aging and investigated the gene chip data of mutator HSCs and their littermate controls for correlation to these genes. As an independent training set, we performed the same analysis on a previously published gene chip data set on young and aged WT HSCs (Chambers et al., 2007). While it displayed highly significant correlation to the aged training set (Figure 5H, left panel), this analysis failed to reveal any significant differences in the gene expression patterns of mutator HSCs and their littermate controls (Figure 5H, right panel). Thus, the molecular features of HSC aging are fundamentally different from those arising as a consequence of accumulating mtDNA mutations.

Taken together, these data revealed a fundamental difference between normal HSC aging and the premature aging phenotypes of mutator HSCs. The lineage skewing associated with normal aging appeared to have an underlying genetic/epigenetic basis at the HSC level, possibly caused by the selective expansion of a class of myeloid-biased HSCs (Figure 5C), but with little evidence of functional alterations that affect mitochondrial

function. By contrast, mutator HSCs displayed a consistently lower MMP (Figure 4), but no apparent differences in global gene expression.

DISCUSSION

The aging blood system experiences profound changes in both the types of effector cells generated as well as the function of produced cells. Combined, such changes lead to a compromise in adaptive immunity, underlie anemia, and cause decreased stress responses (Rossi et al., 2008). Many, if not all, of the changes in hematopoietic regenerative capacity with age are coupled to an altered functional capacity of HSCs, which appear to have multiple mechanistic foundations, including the accumulation of macromolecular damage, epigenetic dysregulation, and/or a clonal selection for myeloid biased cells (Beerman et al., 2010; Chambers et al., 2007; Morales et al., 2005; Nijnik et al., 2007; Rossi et al., 2005, 2007).

In the adult, HSCs remain relatively inactive (Passegue et al., 2005), and most data argue that the primitive compartment of hematopoietic cells that includes HSCs relies more on glycolysis as opposed to OXPHOS as the primary means of ATP synthesis (Simsek et al., 2010; Unwin et al., 2006). However, OXPHOS is only one of many roles executed by mitochondria. By addressing the distribution of mitochondria in highly defined hematopoietic progenitor cells, hypothesizing that mitochondrial numbers might serve as a general indicator of the cellular dependence of various mitochondrial processes, we exposed different levels of mitochondria as a result of early hematopoietic differentiation. Importantly, among the primitive subsets studied, HSCs carry relatively high levels of mitochondria, although these are less active, at least when evaluating MMP.

Mice with defective mitochondrial polymerase gamma ("mutator" mice) exhibit multiple premature aging phenotypes, including osteoporosis, weight loss, thymic involution, and anemia (Trifunovic et al., 2004). These phenotypes arise gradually along with accumulating mitochondrial mutations. Here we identified several defined developmental stages in hematopoiesis, where the mutator genotype leads to prominent perturbations, including an increase/block of early erythropoiesis (at the pre CFU-E stage) and a reduction of B cell committed progenitor cells (ProB) (Figure 2). However, HSC frequencies of mutator mice did not diverge from those of wild-type mice, evidenced further by an intact production of myeloid cells, which has previously been demonstrated to serve as a good indicator of maintained HSC function (Domen et al., 2000). Therefore, individual hematopoietic lineages call upon separate mechanisms in order to fulfill the metabolic requirements required for their appropriate differentiation. Hence, the bottlenecks in differentiation caused by insufficient mitochondrial function are traceable to defined stages of hematopoietic development. This situation appears very similar to differentiation of embryonic stem cells, where differentiation is accompanied by an in initial decrease followed by a rapid increase in mitochondrial numbers, which correlate with an increased OXPHOS dependence (Facucho-Oliveira and St John, 2009).

Although it has previously demonstrated that mutator mice associate with a high mitochondrial DNA mutation load, it is also clear that this mutational load differs between tissues (Vermulst et al., 2007). As we demonstrate here, pre CFU-Es, which are severely affected by the mutator genotype (Figure 2C), display a mutation load very similar to that of HSCs (Figure 4A). Although this demonstrates that HSCs do indeed succumb to accumulation of mitochondrial DNA mutations in mutator mice, our data do not exclude the possibility that HSCs are, to some extent, guarded against the accumulation of mitochondrial mutations due to their relative quiescence or glycolytic metabolism. Alternatively, or complementary, it might also well be that the mutation load varies depending on the proliferation properties of the tissue, with the blood system representing a highly proliferative tissues, whereas previous studies have mainly focused on postmitotic tissues such as cardiac muscle or neurons of the brain.

Eosinophils generate their MMP through hydrolysis of ATP rather than from oxidative respiration. Therefore, treatment with the F_0/F_1 ATPase inhibitor Oligomycin does not result in increased MMP of such cells (Peachman et al., 2001), akin to what we observed for mutator pre CFU-Es. However, despite the absence of respiration observed in eosinophils, their mitochondria actively participate in the regulation of apoptosis (Peachman et al., 2001). We hypothesized that pre CFU-Es were highly reliant on mitochondrial respiration for ATP synthesis given the extent of their perturbation in mutator mice and based on their high-level expression of nuclear genes of the OXPHOS chain (Figure S4). We did, however, fail to observe a difference in intracellular ATP levels between mutator and WT pre CFU-Es (Figure 4C), somewhat in contrast to previous studies on mutator cells (Hiona et al., 2010; Trifunovic et al., 2004). Although our studies do not exclude the possibility that mutator pre CFU-Es display a reduced ATP synthesis by OXPHOS and are able to compensate by, for instance, anaerobic glycolysis, we rather favor that, in contrast to a postmitotic tissue such as muscle, the blood is a highly mitotic tissue that relies on constant output of progenitor cells throughout life. Therefore, as mitochondrial mutations accumulate, progenitor cells that rely on intact mitochondrial function will be unable to proliferate/differentiate, subsequently be eliminated, and therefore not present with noticeable differences in ATP levels when evaluated in vivo.

Several genetically modified animals that model physiological aging are available and have been the subject of intense study (Morales et al., 2005; Nijnik et al., 2007; Rossi et al., 2007). However, common for most, if not all, of these model animals is that they fail to mimic the multifactorial aspects of aging. The validity of mutator mice as a model-system for physiological aging can be questioned as accumulation of mtDNA mutations in this strain has been shown to be more than a magnitude higher when compared to various human tissue from aged individuals (Khrapko et al., 2006). Additionally, another mutator strain failed to recreate the multiple aspects of normal skeletal muscle aging (Hiona et al., 2010). In agreement with this, while mimicking certain phenotypes associated with HSC aging, including development of lymphopenia and anemia, a distinct functional discrepancy emerges between HSC activity of mutator mice and that of physiologically aged HSCs, evidenced by the absence of a molecularly aged phenotype and epigenetic alteration of mutator HSCs (Figure 5). Although this does not exclude that mitochondrial mutations are a contributing factor in physiological aging, our studies do demonstrate that severe

mitochondrial mutations, to a large extent, fail to promote HSC-aging phenotypes despite having staggering consequences at distinct downstream progenitor levels. Our data therefore highlight the importance of probing mitochondrial integrity and function, combined with exploration of mitochondria-based therapies, in the development of therapeutic modalities based on HSCs.

EXPERIMENTAL PROCEDURES

Mice

Two- to nine-month-old heterozygous Polg^{tm1Lrsn} mice (a kind gift from Nils-Göran Larsson; Trifunovic et al., 2004) were backcrossed with CD45.1$^+$ C57BL/6 mice for four generations. Littermate siblings were used as controls throughout these studies. For some experiments not involving mutator mice (in Figure 1 and Figure 5), young (10–12 weeks) or aged (24 months) C57BL/6J were used. All mice procedures were performed with consent from the local ethics committee.

Immunophenotypic Analysis and Cell Sorting

Isolation and analysis of hematopoietic stem cells and lymphoid progenitors by FACS were performed as described (Inlay et al., 2009; Pronk and Bryder, 2011; Pronk et al., 2007). Myeloid-biased Slamf1^{hi} HSCs (Figure 5) were identified as described (Beerman et al., 2010). Cells were sorted and analyzed on a FACS Aria cell sorter (Becton Dickinson, Franklin Lakes, NJ). All flow cytometry and FACS data were analyzed with FlowJo software (Treestar, Ashland, OR).

Peripheral Blood

Peripheral blood was collected from the tail vein in Microvette tubes (Sarstedt, Nürmbrecht, Germany) and analyzed on a Sysmex KX-21 N machine (Sysmex, Norderstedt, Germany).

In Vivo Reconstitution Experiments

Competitive repopulation experiments using the congenic CD45.1/CD45.2 mouse model were performed as described previously (Pronk et al., 2007). For reconstitution analysis of transplanted recipients, chimerism was calculated as the percentage of donor contribution within the specified lineages. Bone marrow HSC chimerism levels were evaluated similarly by individual isolation of BM cells from each recipient followed by staining for HSC and progenitor markers, in addition to antibodies against CD45.1 and CD45.2 to distinguish test cells from competitor cells/host cells.

For serial transplantation experiments, 10^6 unfractionated BM cells from mutator mice or their wild-type littermate controls were transplanted into irradiated C57BL/6 hosts. Sixteen weeks after transplantation, HSCs (Lin$^-$Sca1$^+$ckit$^+$CD34$^{-/lo}$CD150$^+$) were isolated from the bone marrow of primary recipient and transplanted at 500 cells/mouse together with 300,000 C57BL/6 bone marrow cells.

CFU-S8 capacity of FACS sorted pre Meg/E cells was evaluated as described (Pronk et al., 2007).

In Vitro Culture Assays

Freshly isolated hematopoietic stem and progenitor cells were cultured in standard culture conditions (37°C, 98% humidity, and 5% CO_2) in OptiMEM (Invitrogen, Carlsbad, CA) supplemented with 10% FCS in the presence of SCF (50 ng/ml), IL3 (10 ng/ml, Peprotech Inc.), and erythropoietin (EPO; 5 U/ml; Janssen-Cilag, Bersee, Belgium) to evaluate clonogenic activity and lineage potentials of isolated cell populations. Myeloid and B cell potential of GMLPs was evaluated by sorting GMLPs directly onto OP9 stromal supported cultures, as described (Pronk et al., 2008). Pre CFU-Es were sorted and cultured in OptiMEM supplemented with 10% FCS in the presence of SCF (50 ng/ml), IL3 (10 ng/ml), and EPO (5 U/ml). Total cell numbers were counted after 3 days of culture to calculate erythroid output. For apoptosis assays, cells were sorted and cultured in OptiMEM supplemented with 10% FCS in the presence of SCF (50 ng/ml), IL3 (10 ng/ml), and EPO (5 U/ml) as above. After culture, cells were incubated with Annexin V (Becton Dickinson, Franklin Lakes, NJ) and Propidium Iodide (Invitrogen, Carlsbad, CA) according to manufacturer's instructions and directly evaluated by flow cytometry to obtain the frequency of Annexin V-positive cells.

ROS Assay

ROS levels were measured in ckit-enriched bone marrow cells (MACS, Miltenyi Biotech, Bergisch Gladbach, Germany) stained with antibodies to define HSCs and progenitors. Cells were subsequently incubated in 5 μM DCFH-DA (Invitrogen, Carlsbad, CA) for 30 min at 37°C and analyzed by FACS immediately after staining.

ATP Quantification

ATP was quantified using the ATP bioluminescent somatic cell assay kit (Sigma-Aldrich, St. Louis, MO) following manufacturer's recommendations. In short, cells were sorted into PBS and 3.9×10^{-13} moles of ATP standard was added to standard samples. Directly following isolation, cells were incubated with the ATP releasing agent (Sigma-Aldrich, St. Louis, MO) and illumination was immediately quantified with a Glomax Illuminator (Promega, Madison, WI).

Mitochondrial Quantification and mtDNA Sequencing

Cells were sorted into lysis buffer containing Proteinase K and incubated at 50°C for 60 min followed by 4 min at 99°C. Samples were diluted in water and subjected to quantitative PCR as described (Attema et al., 2009) with primers directed against genomic or mitochondrial DNA using MyiQ iCycler (Biorad, Hercules, CA). For mtDNA sequencing, single cells were sorted and treated as above, following PCR amplification with primers directed against mtDNA (Fw: 5′-GTTATTAGGGTGGCAGAGCCAG-3′, Rev: 5′-GCCCGATAG CTTAATTAGCTGAC-3′; region 2673–3873, GenBank: V00711) and Phusion Hot Start II High-Fidelity Polymerase (Thermo Fisher, Waltham, MA). PCR amplified fragments were thereafter purified and sequenced by Eurofins MWG Operon (Ebersberg, Germany).

For mitochondrial quantification by FACS, bone marrow cells were stained with antibodies to define HSCs and progenitors. Cells were subsequently stained in the presence of 50 μM Verapamil (Sigma-Aldrich, St. Louis, MO) with 20 nM MitoTracker Green (Invitrogen, Carlsbad, CA) according to manufacturer's recommendations and analyzed by FACS immediately after staining.

Membrane Potential Evaluation

Mitochondrial membrane potential was evaluated in bone marrow samples depleted of cells positive for lineage markers and enriched for cells expressing ckit. Following antibody staining to identify HSCs and progenitors, cells were incubated in OptiMem supplemented with 10% FCS in the presence of SCF (10 ng/ml), TPO (10 ng/ml), and IL3 (5 ng/ml) for 3 hr at standard culture conditions. Following 2 hr in culture, selected samples were cultured for 1 hr in the presence of 5 μg/ml Oligomycin (Sigma-Aldrich, St. Louis, MO) or for 5 min in 5 μM carbonyl cyanide 3-chlorophenylhydrazone (CCCP) (Sigma-Aldrich, St. Louis, MO). Subsequently, all samples were incubated in the presence of 5 μM Verapamil for 10 min, after which samples were stained with the lipophilic, cationic dye JC-1 (Cayman Chemical Company, Ann Arbor, MI) at 1/1000 dilution according to manufacturer's recommendations, followed by FACS analysis.

Affymetrix Gene Expression Analysis and Quantitative RT-PCR

RNA was extracted in triplicates for each group from 4000–7000 HSCs with RNeasy-micro mRNA purification kit (QIAGEN), as previously described (Pronk et al., 2007). Subsequent handling was performed at the Stanford PAN facility (http://cmgm.stanford.edu/pan/). The microarray data in Figure 1B and Figure S4 can be found in the Gene Expression Omnibus (Pre Meg/E, Pre CFU-E, CFU-E, MkP and CLP, accession number GSE8407) (GMLP, accession number GSE18734) (ProB, accession number GSE14833) and the Training Set Data in Figure 5D (accession number GSE6503).

For subsequent analysis, probe level expression values were extracted using RMA and analyses were done using dChip software (http://biosun1.harvard.edu/complab/dchip/) following filtering out probes with a lower expression than 100 in all subsets to eliminate noise in expression.

Quantitative RT-PCR experiments were performed as described (Attema et al., 2009).

Expression profiles of each subset were analyzed for correlation to a 140 gene-aging list using Gene Set Enrichment Analysis (Subramanian et al., 2005).

Statistics

Results were statistically analyzed and figures prepared using Excel and GraphPad Prism (GraphPad Inc.) software. A two-tailed Student's t test was used throughout to evaluate statistical significance. Significance is indicated as follows: *$p < 0.05$, **$p < 0.001$, and ***$p < 0.0001$.

ACCESSION NUMBERS

The GEO accession numbers for the microarray data reported in this paper are GSE8407, GSE18734, GSE14833, GSE6503, GSE27686, and V00711.

SUPPLEMENTAL INFORMATION

Supplemental Information includes four figures, one table, and Supplemental Experimental Procedures and can be found with this article online at doi:10.1016/j.stem.2011.03.009.

ACKNOWLEDGMENTS

We gratefully acknowledge N.-G. Larsson for making mutator mice available, T. Suda for details on ATP measurements, and the Stanford PAN facility for help with microarray experiments. The work was supported by grants to D.B. from the Swedish Cancer Foundation, the Swedish Medical Research Council, the Swedish Pediatric Leukemia Foundation, and the Crafoord Foundation. G.L.N., C.J.P. and D.B. designed studies. All authors contributed to experiments. D.B. and G.L.N. wrote the manuscript.

Received: November 12, 2010
Revised: February 12, 2011
Accepted: March 11, 2011
Published: May 5, 2011

REFERENCES

Allsopp, R.C., Cheshier, S., and Weissman, I.L. (2001). Telomere shortening accompanies increased cell cycle activity during serial transplantation of hematopoietic stem cells. J. Exp. Med. *193*, 917–924.

Attema, J.L., Pronk, C.J., Norddahl, G.L., Nygren, J.M., and Bryder, D. (2009). Hematopoietic stem cell ageing is uncoupled from p16 INK4A-mediated senescence. Oncogene *28*, 2238–2243.

Beerman, I., Bhattacharya, D., Zandi, S., Sigvardsson, M., Weissman, I.L., Bryder, D., and Rossi, D.J. (2010). Functionally distinct hematopoietic stem cells modulate hematopoietic lineage potential during aging by a mechanism of clonal expansion. Proc. Natl. Acad. Sci. USA *107*, 5465–5470.

Chambers, S.M., Shaw, C.A., Gatza, C., Fisk, C.J., Donehower, L.A., and Goodell, M.A. (2007). Aging hematopoietic stem cells decline in function and exhibit epigenetic dysregulation. PLoS Biol. *5*, e201.

Chaudhary, P.M., and Roninson, I.B. (1991). Expression and activity of P-glycoprotein, a multidrug efflux pump, in human hematopoietic stem cells. Cell *66*, 85–94.

Chen, M.L., Logan, T.D., Hochberg, M.L., Shelat, S.G., Yu, X., Wilding, G.E., Tan, W., Kujoth, G.C., Prolla, T.A., Selak, M.A., et al. (2009). Erythroid dysplasia, megaloblastic anemia, and impaired lymphopoiesis arising from mitochondrial dysfunction. Blood *114*, 4045–4053.

Domen, J., Cheshier, S.H., and Weissman, I.L. (2000). The role of apoptosis in the regulation of hematopoietic stem cells: Overexpression of Bcl-2 increases both their number and repopulation potential. J. Exp. Med. *191*, 253–264.

Facucho-Oliveira, J.M., and St John, J.C. (2009). The relationship between pluripotency and mitochondrial DNA proliferation during early embryo development and embryonic stem cell differentiation. Stem Cell Rev. *5*, 140–158.

Falkenberg, M., Larsson, N.G., and Gustafsson, C.M. (2007). DNA replication and transcription in mammalian mitochondria. Annu. Rev. Biochem. *76*, 679–699.

Fontenay, M., Cathelin, S., Amiot, M., Gyan, E., and Solary, E. (2006). Mitochondria in hematopoiesis and hematological diseases. Oncogene *25*, 4757–4767.

Gogvadze, V., Orrenius, S., and Zhivotovsky, B. (2006). Multiple pathways of cytochrome c release from mitochondria in apoptosis. Biochim. Biophys. Acta *1757*, 639–647.

Goodell, M.A., Rosenzweig, M., Kim, H., Marks, D.F., DeMaria, M., Paradis, G., Grupp, S.A., Sieff, C.A., Mulligan, R.C., and Johnson, R.P. (1997). Dye efflux studies suggest that hematopoietic stem cells expressing low or undetectable levels of CD34 antigen exist in multiple species. Nat. Med. *3*, 1337–1345.

Harman, D. (1972). The biologic clock: the mitochondria? J. Am. Geriatr. Soc. *20*, 145–147.

Harrison, D.E. (1980). Competitive repopulation: a new assay for long-term stem cell functional capacity. Blood *55*, 77–81.

Harrison, D.E., Astle, C.M., and Delaittre, J.A. (1978). Loss of proliferative capacity in immunohemopoietic stem cells caused by serial transplantation rather than aging. J. Exp. Med. *147*, 1526–1531.

Hiona, A., Sanz, A., Kujoth, G.C., Pamplona, R., Seo, A.Y., Hofer, T., Someya, S., Miyakawa, T., Nakayama, C., Samhan-Arias, A.K., et al. (2010). Mitochondrial DNA mutations induce mitochondrial dysfunction, apoptosis and sarcopenia in skeletal muscle of mitochondrial DNA mutator mice. PLoS ONE *5*, e11468.

Huttemann, M., Lee, I., Pecinova, A., Pecina, P., Przyklenk, K., and Doan, J.W. (2008). Regulation of oxidative phosphorylation, the mitochondrial membrane potential, and their role in human disease. J. Bioenerg. Biomembr. *40*, 445–456.

Inlay, M.A., Bhattacharya, D., Sahoo, D., Serwold, T., Seita, J., Karsunky, H., Plevritis, S.K., Dill, D.L., and Weissman, I.L. (2009). Ly6d marks the earliest stage of B-cell specification and identifies the branchpoint between B-cell and T-cell development. Genes Dev. *23*, 2376–2381.

Khrapko, K., Kraytsberg, Y., de Grey, A.D., Vijg, J., and Schon, E.A. (2006). Does premature aging of the mtDNA mutator mouse prove that mtDNA mutations are involved in natural aging? Aging Cell *5*, 279–282.

Kollman, C., Howe, C.W., Anasetti, C., Antin, J.H., Davies, S.M., Filipovich, A.H., Hegland, J., Kamani, N., Kernan, N.A., King, R., et al. (2001). Donor characteristics as risk factors in recipients after transplantation of bone marrow from unrelated donors: the effect of donor age. Blood *98*, 2043–2051.

Kujoth, G.C., Hiona, A., Pugh, T.D., Someya, S., Panzer, K., Wohlgemuth, S.E., Hofer, T., Seo, A.Y., Sullivan, R., Jobling, W.A., et al. (2005). Mitochondrial DNA mutations, oxidative stress, and apoptosis in mammalian aging. Science *309*, 481–484.

Larsson, N.G. (2010). Somatic mitochondrial DNA mutations in mammalian aging. Annu. Rev. Biochem. *79*, 683–706.

Marques-Santos, L.F., Oliveira, J.G., Maia, R.C., and Rumjanek, V.M. (2003). Mitotracker green is a P-glycoprotein substrate. Biosci. Rep. *23*, 199–212.

Morales, M., Theunissen, J.W., Kim, C.F., Kitagawa, R., Kastan, M.B., and Petrini, J.H. (2005). The Rad50S allele promotes ATM-dependent DNA damage responses and suppresses ATM deficiency: implications for the Mre11 complex as a DNA damage sensor. Genes Dev. *19*, 3043–3054.

Nijnik, A., Woodbine, L., Marchetti, C., Dawson, S., Lambe, T., Liu, C., Rodrigues, N.P., Crockford, T.L., Cabuy, E., Vindigni, A., et al. (2007). DNA repair is limiting for haematopoietic stem cells during ageing. Nature *447*, 686–690.

Passegue, E., Wagers, A.J., Giuriato, S., Anderson, W.C., and Weissman, I.L. (2005). Global analysis of proliferation and cell cycle gene expression in the regulation of hematopoietic stem and progenitor cell fates. J. Exp. Med. *202*, 1599–1611.

Peachman, K.K., Lyles, D.S., and Bass, D.A. (2001). Mitochondria in eosinophils: functional role in apoptosis but not respiration. Proc. Natl. Acad. Sci. USA *98*, 1717–1722.

Pronk, C.J., and Bryder, D. (2011). Flow cytometry-based identification of immature myeloerythroid development. Methods Mol. Biol. *699*, 275–293.

Pronk, C.J., Rossi, D.J., Mansson, R., Attema, J.L., Norddahl, G.L., Chan, C.K., Sigvardsson, M., Weissman, I.L., and Bryder, D. (2007). Elucidation of

the phenotypic, functional, and molecular topography of a myeloerythroid progenitor cell hierarchy. Cell Stem Cell *1*, 428–442.

Pronk, C.J., Attema, J., Rossi, D.J., Sigvardsson, M., and Bryder, D. (2008). Deciphering developmental stages of adult myelopoiesis. Cell Cycle *7*, 706–713.

Rossi, D.J., Bryder, D., Zahn, J.M., Ahlenius, H., Sonu, R., Wagers, A.J., and Weissman, I.L. (2005). Cell intrinsic alterations underlie hematopoietic stem cell aging. Proc. Natl. Acad. Sci. USA *102*, 9194–9199.

Rossi, D.J., Bryder, D., Seita, J., Nussenzweig, A., Hoeijmakers, J., and Weissman, I.L. (2007). Deficiencies in DNA damage repair limit the function of haematopoietic stem cells with age. Nature *447*, 725–729.

Rossi, D.J., Jamieson, C.H., and Weissman, I.L. (2008). Stems cells and the pathways to aging and cancer. Cell *132*, 681–696.

Simsek, T., Kocabas, F., Zheng, J., Deberardinis, R.J., Mahmoud, A.I., Olson, E.N., Schneider, J.W., Zhang, C.C., and Sadek, H.A. (2010). The distinct metabolic profile of hematopoietic stem cells reflects their location in a hypoxic niche. Cell Stem Cell *7*, 380–390.

Subramanian, A., Tamayo, P., Mootha, V.K., Mukherjee, S., Ebert, B.L., Gillette, M.A., Paulovich, A., Pomeroy, S.L., Golub, T.R., Lander, E.S., et al. (2005). Gene set enrichment analysis: a knowledge-based approach for interpreting genome-wide expression profiles. Proc. Natl. Acad. Sci. USA *102*, 15545–15550.

Trifunovic, A., Wredenberg, A., Falkenberg, M., Spelbrink, J.N., Rovio, A.T., Bruder, C.E., Bohlooly, Y.M., Gidlof, S., Oldfors, A., Wibom, R., et al. (2004). Premature ageing in mice expressing defective mitochondrial DNA polymerase. Nature *429*, 417–423.

Unwin, R.D., Smith, D.L., Blinco, D., Wilson, C.L., Miller, C.J., Evans, C.A., Jaworska, E., Baldwin, S.A., Barnes, K., Pierce, A., et al. (2006). Quantitative proteomics reveals posttranslational control as a regulatory factor in primary hematopoietic stem cells. Blood *107*, 4687–4694.

Vermulst, M., Bielas, J.H., Kujoth, G.C., Ladiges, W.C., Rabinovitch, P.S., Prolla, T.A., and Loeb, L.A. (2007). Mitochondrial point mutations do not limit the natural lifespan of mice. Nat. Genet. *39*, 540–543.

Wong, A., and Cortopassi, G. (2002). Reproducible quantitative PCR of mitochondrial and nuclear DNA copy number using the LightCycler. Methods Mol. Biol. *197*, 129–137.